Effect of Strakes on the aerodynamic characteristics of the circular cylinder and its effect on the vortex shedding [a)]

S Nadaraja Pillai,[1,b)] Karthik Vel E,[1)] Ranga Srinivas Gokul,[1)] Rohinth U,[1)] and Abhishek S, [1)]

[1]*Turbulence & flow control laboratory, School of Mechanical Engineering, SASTRA deemed to be University, Thanjavur, Tamil Nadu-613401, India*

.

ABSTRACT

This experimental investigation was performed over the baseline circular cylinder and the cylinder attached with helical strakes of different pitches and diameters around a circular cylinder. Time series pressure data is measured from all over the cylinder surface utilising a simultaneous pressure scanner with 64 channels. The investigation aims to suppress vortex-induced vibration (VIV) over a circular cylinder by employing helical strakes of a circular cross-section with varying pitch and diameter. The pitch ratio of the strakes varied from 0.5,1 and 2 and correspondingly the diameter ratio of 0.03,0.04,0.1 and 0.13. The study presents conclusive evidence, utilising the surface pressure data to demonstrate the effectiveness of helical strakes in mitigating the aerodynamic drag characteristics and suppressing VIV. The findings of this study have significant implications for the design of structures such as lamp posts, chimneys, towers, cables, high-rise building supports, bridge support and offshore structures, as the unsteady fluid flow around such structures will cause a non-uniform aerodynamic force which in turn results in unsteady shedding. The use of helical strakes is found to be one of the appropriate Passive flow control devices for suppressing the non-uniform shedding occurring downstream of the cylinder.

I. INTRODUCTION:

Cylindrical structures are a classic example of an aerodynamically bluff body. The range of applications of cylindrical structures is huge, including but not limited to turbine shafts, cables, support poles, struts etc. Though aerodynamically inefficient, these structures are implemented to offer a higher torsional rigidity in structural application. A main classifier for a bluff body is that the aerodynamic drag is mostly constituted by the pressure drag component. This behaviour can be attributed to a heavier magnitude of distortion to the incoming streamline, causing the formation of a shear layer. The aerodynamic characteristics of a cylinder have been analysed in depth, with detailed specifics on the behaviour at critical, subcritical and post-critical Re regimes. The vorticity build-up in the shear layer, combined with boundary layer separation produces a time-series, continuous phenomena of vortex shedding. Vortices are continuously shed at a constant frequency, determined by the Strouhal number (St). This phenomenon is well observed for subcritical, lower Re (Reynolds number) regimes, forming a

[a] The International Conference on Recent Advances in Fluid Mechanics and Nanoelectronics (ICRAFMN – 2023) hosted by Manipal Institute of Technology (MIT) Bengaluru in association with NIT Uttarakhand from 12th -14th July 2023 at MIT Bengaluru

[b] Corresponding author: Electronic email: *nadarajapillai@mech.sastra.edu*

vortex street. Turbulent separation at critical and post-critical regimes suppresses the vortices, producing a turbulent vortex street. This turbulent vortex street is well observed in the ranges of 1.5 to 3×10^5. Vortex-induced vibrations cause heavy structural damage and induce creep stress in the base structure. This phenomenon is detrimental to cylindrical structures in both hydrodynamic and aerodynamic applications, so when the cylinder is flexible or supported like in the case of factory chimneys, VIV could be excited under the complex interaction between the shedding vortices and the structural elasticity (Williamson and Govardhan[1]; Paidoussis et al.[2]). The flow physics of the wakes caused by the bluff bodies and the complex three dimensional and oscillatory behaviour due to periodic vortex shedding is reviewed in detail[3].It has been found that this VIV could create a phenomenon called lock-in/synchronization (Feng,[4]). A passive method to control such vibrations would be the implantation of helical strakes, wherein turbulence is induced such that the flow momentum increases, causing delayed separation. The passive method of implementing the slots in the cylinder cross-section has delayed flow separation and increased the surface vorticity by 3% to 26.4% further increasing the bubble length by 0.7% to 6.75%[5].Certain, Active methods were utilised to control the growth of the wake in downstream of the bluff bodies thereby reducing the drag force, methods implementing linear and sawtooth plasma actuators in the steady and unsteady modes have a maximum drag reduction of 58% and 22.8% [6]. Experimental investigation incorporating the Dielectric plasma actuator at the natural separation point pulsed at a frequency greater than 0.6 has resulted in the suppression of the vortex shedding and increased drag reduction [7]. The squared cylinder's downstream surface jet injection has resulted in a decrease in pressure coefficients at the upstream and an increase at the downstream surfaces. Therefore, there was a considerable drop of 26%, 33%, and 38% in the drag coefficients [8].The efficiency of using helical strakes has been extensively studied by T. Zhou[9], complete with the optimum basic pitch and diameter ratios. Computational simulation through DES was carried out by Nicholas. P.Jones et al.[10] at post-critical Reynolds number regimes. The acoustic implications of utilizing strakes, dealing with the tonal noise utilizing permeable materials as listed by Geyer et al.[11] also include the reduction in mean velocity. Vortex-induced vibrations are not wholly detrimental, with Gabriel et al.[12] implementing an energy harvesting system from non-linear energy sinks (NES). Dai et al.[13] have also given a different approach to energy harvest utilizing a piezoelectric-based energy harvesting system. A study on energy harvesting of vortex-induced vibrations based on nonlinear damping was also conducted (Baoshou Zhang,[14]).It proved that nonlinear damping increased the vibrational power compared to constant damping. Zeinoddini et al.[15] provided a conclusive study on the cross-flow implications. The implications of implementing strakes, as given by Bearman [16] shown that shedding is not effectively reduced for smaller strakes and the prevention of separated shear layer interactions. Also, it was unclear about the efficiency of strakes in a recently discovered bidirectional shear flow.(Xuepeng Fu,[17]), conducted an experimental study on the Vortex-induced vibration of a straked pipe subjected to bidirectionally sheared flow and concluded that strakes are indeed

efficient in suppressing the vibrations and reducing fatigue damage by over 99%. The scope of this experimental study is to analyse and present the effects of implementing circular strakes of varying D_r (diameter ratio) and P_r (pitch ratio). A brief investigation is also carried out at induced turbulence levels. This VIV is also a huge problem for stay cables used in bridges, The first report was made by (Hikami and Shiraishi,)[18,19]. A computational study on aerodynamic mitigation of large amplitude vibrations on stay cables was done [10]**.** However, without a thorough grasp of the underlying principles causing the vibrations caused by the wind, such countermeasures cannot be successful. The two types of excitation processes that have been proposed so far by different researchers are galloping instability and high-speed vortex-induced vibration. The former is connected to a response with a velocity restriction (Matsumoto et al.)[20,21]. and the latter is related to flow instability due to water rivulets [18] or cable inclination [22]. There were also various numerical investigations involving vortex-induced vibrations, one such paper a numerical investigation of the suppression of "Vortex-Induced Vibration" (VIV) of a cylindrical flexible riser to which are attached various grooved or strip configurations with the ensemble exposed to uniform flow. The result showed that cylindrical or grooved risers with different strip configurations are used to improve VIV suppression [23]. The purpose of this work was to suggest the creation of a method for efficiently disrupting the three-dimensional flow structures that produce the low-frequency forces, using a strake pattern that is appropriately designed. A numerical study by (Takeshi Ishihara)[24] concluded that lift force fluctuations were significantly reduced for the wired cylinder as the helical wires enhance the three-dimensional disturbances to the wake. Another numerical study by (Decheng Wan)[25] showed that symmetric strips around the cylinder dampen the effect of three-dimensional flow, Consequently, at higher reduced velocities, the transition from VIV to galloping and pure galloping is triggered.

As previously stated, researchers have conducted significant research on the aerodynamic characteristics and the vortex-induced vibration (VIV) analysis on cylindrical structures. However, the study on passive flow control devices on such cylindrical structures has also been extensively discussed without changing the basic structure. The aerodynamic and the shedding characteristics study on cylindrical structures with strakes with various diameters and pitch ratios has to be further well understood. This motivated the current study to investigate the aerodynamic and the shedding characteristics of the cylinder attached to the strakes based on the time series surface pressure data obtained through the pressure ports present along various span-wise locations and the wake rake at the immediate wake of the cylinder. The paper is organized as follows, a brief formulation of the methodology implanted, a presentation of the results and the conclusions drawn from the discussed results.

II. EXPERIMENTAL METHODOLOGY

A. FORMULATION

The effect of the strakes on the aerodynamic characteristics of circular cylinders is experimentally investigated in this current study. The variation of strake diameter and the helical placement of the strakes are characterised by the parameter called diameter ratio (D_r) and the pitch ratio (P_r). The parameters are varied and its effects on the variation of aerodynamic characteristics are studied in detail. The Diameter ratio (D_r) is defined as the ratio of the diameter of the cylindrical strake (d) to the diameter of the cylinder (D) shown in equation (1). The Pitch (P) is defined as the helical distance between each winding shown in equation (2), which is varied from 0.5d, 1d and 2d as tabulated in Table II, while the diameter of the strakes varied from 0.0015m, 0.002m,0.005m and 0.007m as tabulated in Table I

$$Diameter\ Ratio\ (D_r) = \frac{Diameter\ of\ the\ strake\ (d)}{Dimater\ of\ the\ cylinder\ (D)} \quad (1)$$

$$Pitch\ Ratio\ (P_r) = \frac{Pitch\ of\ the\ strake\ winding\ (P)}{Dimater\ of\ the\ cylinder\ (D)} \quad (2)$$

Table I The cylinder model attached with strakes and the model specifications

SL No	*The diameter of the strake (d) (m)*	*Diameter of the cylinder (D) (m)*	*Diameter Ratio (D_r)*
1	0.0015	0.05	0.03
2	0.002	0.05	0.04
3	0.005	0.05	0.1
4	0.007	0.05	0.13

Table II The cylinder model attached with strakes and the various pitch specifications used for the investigation

SL No	*The Pitch of the strake (P) (m)*	*Diameter of the cylinder (D) (m)*	*Pitch Ratio (P_r)*
1	0.025	0.05	0.5
2	0.05	0.05	1
3	0.1	0.05	2

An open loop suction type subsonic tunnel is implemented. A cylinder is designed as specified in Fig.1, with pressure taps on the surface to capture the pressure data. The taps are placed at spanwise locations of L/D 1.80, 2.30, 2.80, and 3.75. The spanwise distribution is uneven in capturing the effects of having pressure taps closer and farther away. Each cross-section has 12 pressure ports. A simultaneous multichannel Scanivalve pressure scanner is implemented for the time series measurement

of surface pressure data and the parameters utilized for the measurement are followed from the research study performed by [26,27].

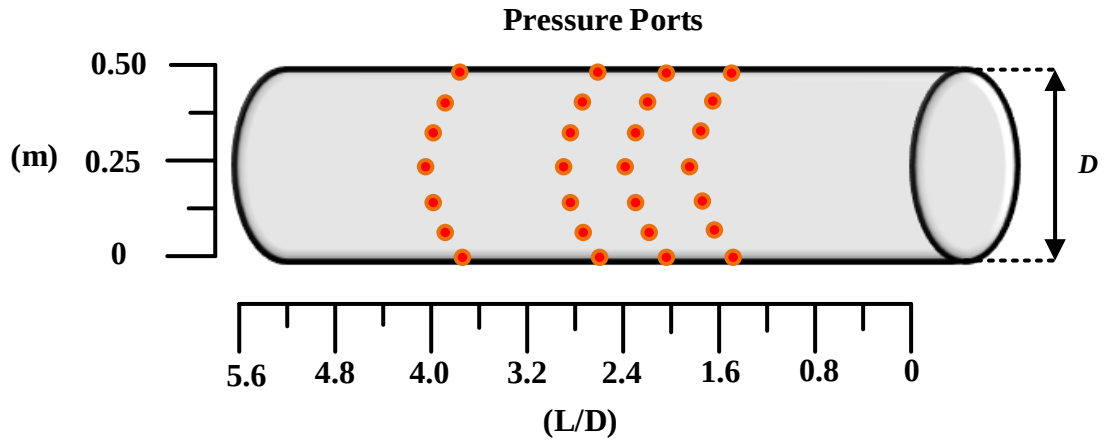

Fig. 1 The Cylinder model with the pressure ports spread across the span-wise direction

Base-Line Model

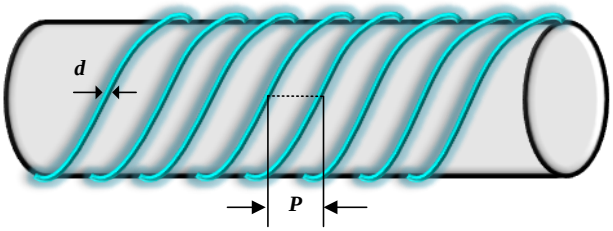

Model 1: P_r =0.5

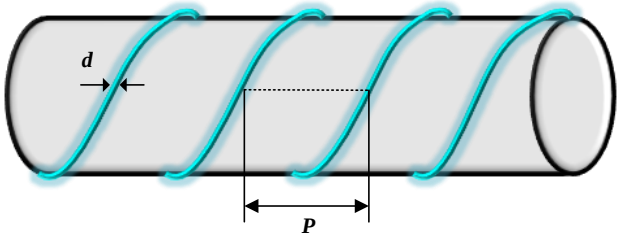

Model 2: P_r =1

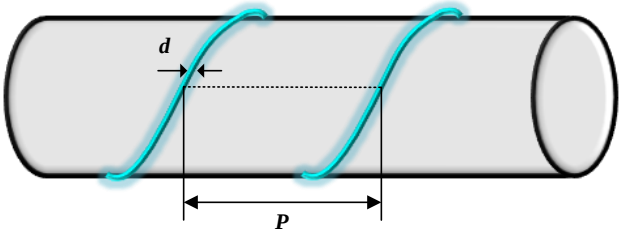

Model 3: P_r =2

Fig. 2 The Cylinder models used for the investigation with three different pitch ratios and varying diameters of the strakes as mentioned in Table I

The experiment is carried out at a velocity of 30m/s, yielding a Re of 1.1×10^5 which is well inside the post-critical regime. As stated by Anderson[28] this regime yields a wholly turbulent vortex street. The C_P distribution over the cylinder is verified for validation and a base model is tested and analysed for shedding and aerodynamic characteristics.

A. PRESSURE MEASUREMENT:

The surface pressure from the pressure ports situated across various spanwise locations of the cylinder is measured by using the ethernet-based MPS pressure scanner, it's a 64-channel simultaneous pressure scanner to which the pressure ports are connected through polyurethane tubings.

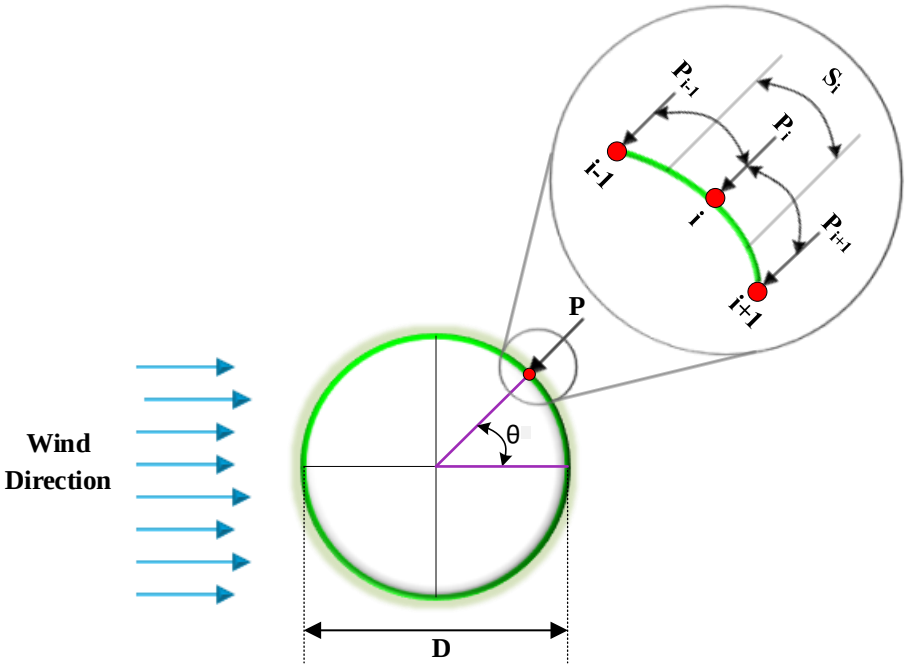

Fig. 3 The Cylinder models used for the investigation with three different pitch ratios and varying diameters of the strakes as mentioned in Table I

The force coefficients have been calculated by integrating the surface pressure across different spanwise cross-sections of the cylinder and an averaged value is obtained for each of the modified models. The aerodynamic force coefficients are computed by integrating the surface pressure across the cylinder cross-section[26,29]. Using Equation. (3) – (6), the overall fluctuating aerodynamic forces were used to compute the aerodynamic coefficient. The static pressure in the free stream is represented as P_∞, and the pressure acting over the i^{th} port is represented as P_i. As illustrated in Fig.3, S_i represents the area that P_i acts on, and θ is the angle that separates the direction of the stream from the normal line to the cylinder's surface at the point of the i^{th} port.

$$D = \sum(P_i - P_\infty) \times S_i \times \cos\theta_i \quad (3)$$

$$L = \sum(P_i - P_\infty) \times S_i \times \sin\theta_i \quad (4)$$

$$C_L = \frac{L}{\frac{1}{2}\times\rho\times V^2\times c} \quad (5)$$

$$C_D = \frac{D}{\frac{1}{2}\times\rho\times V^2\times c} \quad (6)$$

B. SHEDDING CHARACTERISTICS:

An important factor in the analysis of shedding–frequency spectra is the usage of a particular window, specified with a windowing function for a better analysis. The frequency range for vortex shedding, determined via the Strouhal number, approximately yields a theoretical range of around 30 to 120 Hz. A suitable window is chosen and applied, yielding minimum spectral leakage. A MATLAB code was implemented to take the discrete fast Fourier transform (FFT) and subsequently the Power Spectral Density (PSD) of the force data. A suitable window of 2^{11} was utilized since the shedding frequencies can range from 30 Hz to 120 Hz. A Hanning window was utilized with around 1250 frequency bins for one-half of the entire signal, i.e., for 350 Hz. The sampling frequency of 700 Hz was adequate, with a Nyquist frequency of 350 Hz, enabling the effective capturing of frequencies lesser than 350 Hz. Plots between the FFT, and PSD of C_L vs the Strouhal number are analysed (St). The Strouhal number provides a non-dimensional value for the shedding frequency. Subsequent reduction percentages can be calculated utilizing the Strouhal number.

III. RESULTS AND DISCUSSION

A. THE VARIATION OF THE SURFACE PRESSURE COEFFICIENT FOR VARIED PITCH RATIO

Fig.4 represents the coefficient of pressure of the cylinder with the pressure ports spread across the cylinder surface. The colour code represents the baseline and the modified model with the spanwise location of the pressure ports. The base cylinder has shown a decrease in the coefficient of pressure from 1 for the stagnation point ($\theta = 0^o$) to -0.75 ($\theta = 60^o$) which is the local minimum C_P thereafter the pressure increases to a local maximum of -0.68 approximately near the separation point ($\theta = 90^o$) after which it decreases slightly and it becomes constant thereafter in the region between $\theta = 90^o$ to 270^o, the results has a fine agreement with the study by [30]. The surface pressure over the cylinder predominantly ensures the decrease in the pressure on the surface of the cylinder because of the addition of the strake of $D_r = 0.03$. The L/D of 1.80 and 2.50 showed an acceleration of flow over the cylinder due to the favourable pressure gradient and the adverse pressure gradient caused due to the presence of strakes showed an increase in the positive pressure which further delayed the flow separation point which is visible from the L/D =2.50. The increase in the Cp from the local minimum to the local maximum is attributed to the deceleration of flow velocity, promoting the growth of the adverse pressure gradient before the separation point. The plateau in the C_p plot explains the reseparated shear flow and thus creation of a recirculation bubble on the immediate wake of the cylinder. The span-wise C_P plot for the D_r =0.03 and the P_r =0.5 shows that the local minimum C_p values decrease with that of the base model with the maximum difference obtained at L/D =2.50 attributing to the acceleration of the flow. Further, the deacceleration of flow is observed with the induction of the turbulence inside the adverse pressure gradient thereby shifting the flow separation point by

a minimum of 8º to a maximum of 60º. This delay in separation is due to the presence of the strakes which generates turbulence, thereby delaying the development of the adverse pressure gradient and as a result, the drag force and the shedding characteristics of the cylinder with stakes decrease considerably. When we see the influence of the strakes with the increase in the pitch ratio the minimum Cp value decreases further to -0.98 at (θ = 75º) and thereafter it increases to the pressure value of -0.48 at (θ = 120º) for L/D =1.80. However, the variation of the C_p is consistent in the spanwise direction showcasing some spanwise flow influencing the surface pressure, especially at L/D = 2.50.

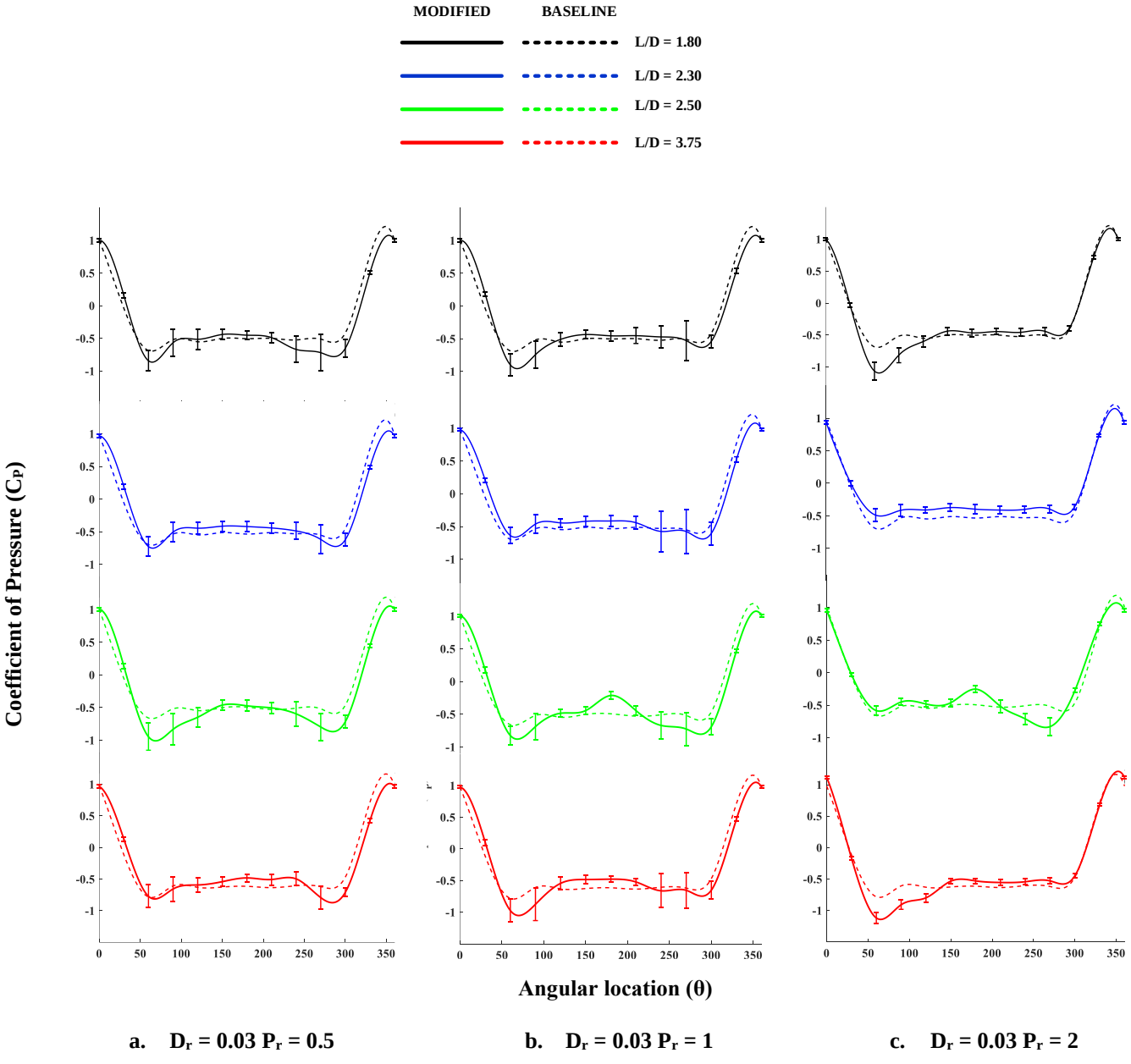

Fig. 4 The Coefficient of pressure (C_P) for the baseline (dotted lines) and modified cylinder with strake model for D_r= 0.03 along four different span-wise locations L/D =1.80,2.30,2.50 and 3.75 and various Pitch ratios a.) P_r = 0.5, b.) P_r = 1 and c.) P_r = 2

The increase in the pitch ratio has delayed the separation point significantly at L/D =1.8 and 3.75 and the effects of the recirculation bubble on the immediate wake are considerably reduced causing the reduction of the effects of shedding from the cylinder surface.

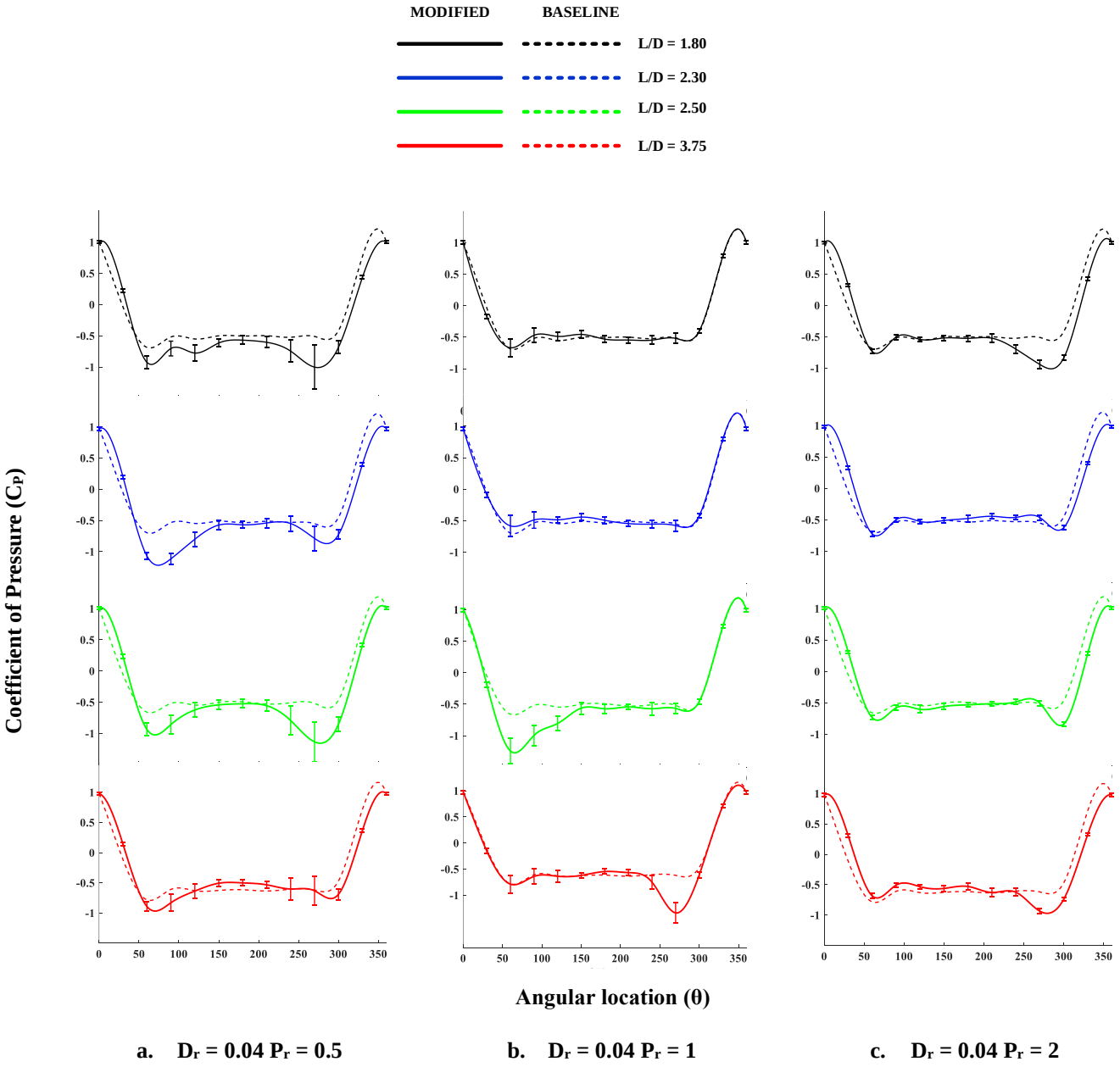

Fig. 5 The Coefficient of pressure (C_P) for the baseline (dotted lines) and modified cylinder with strake model for D_r= 0.04 along four different span-wise locations L/D =1.80,2.30,2.50 and 3.75 and various Pitch ratios a.) P_r = 0.5, b.) P_r = 1 and c.) P_r = 2

Fig. 5 represents the variation of the coefficient of pressure for the cylinder without any strake and the cylinder with the strake for diameter ratio D_r =0.04 and various pitch ratios P_r = 0.5,1 and 2. The local minimum C_p value for the cylinder with D_r =0.04

and the P_r =0.5 is further decreased for almost all the span-wise locations which is attributed to the acceleration of the flow happening for the strake with the increased diameter. The local maximum pressure coefficient for the modified cylinder is almost similar to the baseline model however there is a significant delay in the separation point which is seen throughout the cylinder. The maximum decrease in the pressure coefficient was obtained for the cylinder with the pitch ratio of 0.1, and the plateau was observed to have a source of influence on the surface pressure of the cylinder which therefore has increased the minimum pressure value either in the upper surface of the cylinder or on the lower surface of the cylinder as shown in Fig.5.

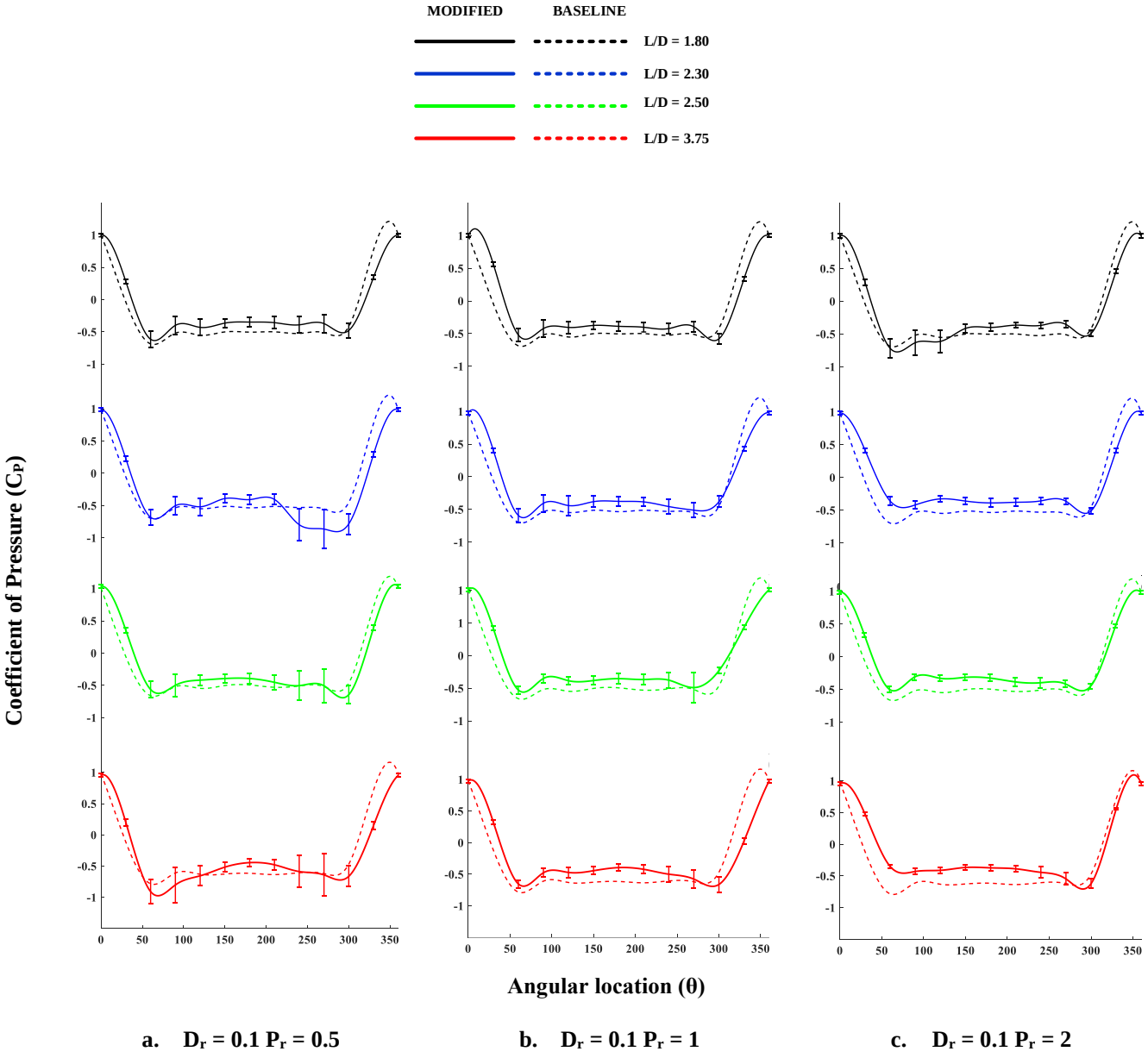

Fig.6 The Coefficient of pressure (C_P) for the baseline (dotted lines) and modified cylinder with strake model for D_r= 0.1 along four different span-wise locations L/D =1.80,2.30,2.50 and 3.75 and various Pitch ratios a.) P_r = 0.5, b.) P_r = 1 and c.) P_r = 2

However, the delay in the separation point is visible from the C_p plot and its variation in the spanwise direction has permitted a significant spanwise flow which has influenced the shedding characteristics reducing wake-induced vibration on the structure.Fig.6 depicts the coefficient of pressure (C_p) for the cylinder model for D_r =0.1 and the various Pitch ratios P_r =0.5,1 and 2. The intersection of the line's tangent to the curve in the regions of constant pressure and adverse pressure gradient yields the separation angle from the pressure plot.

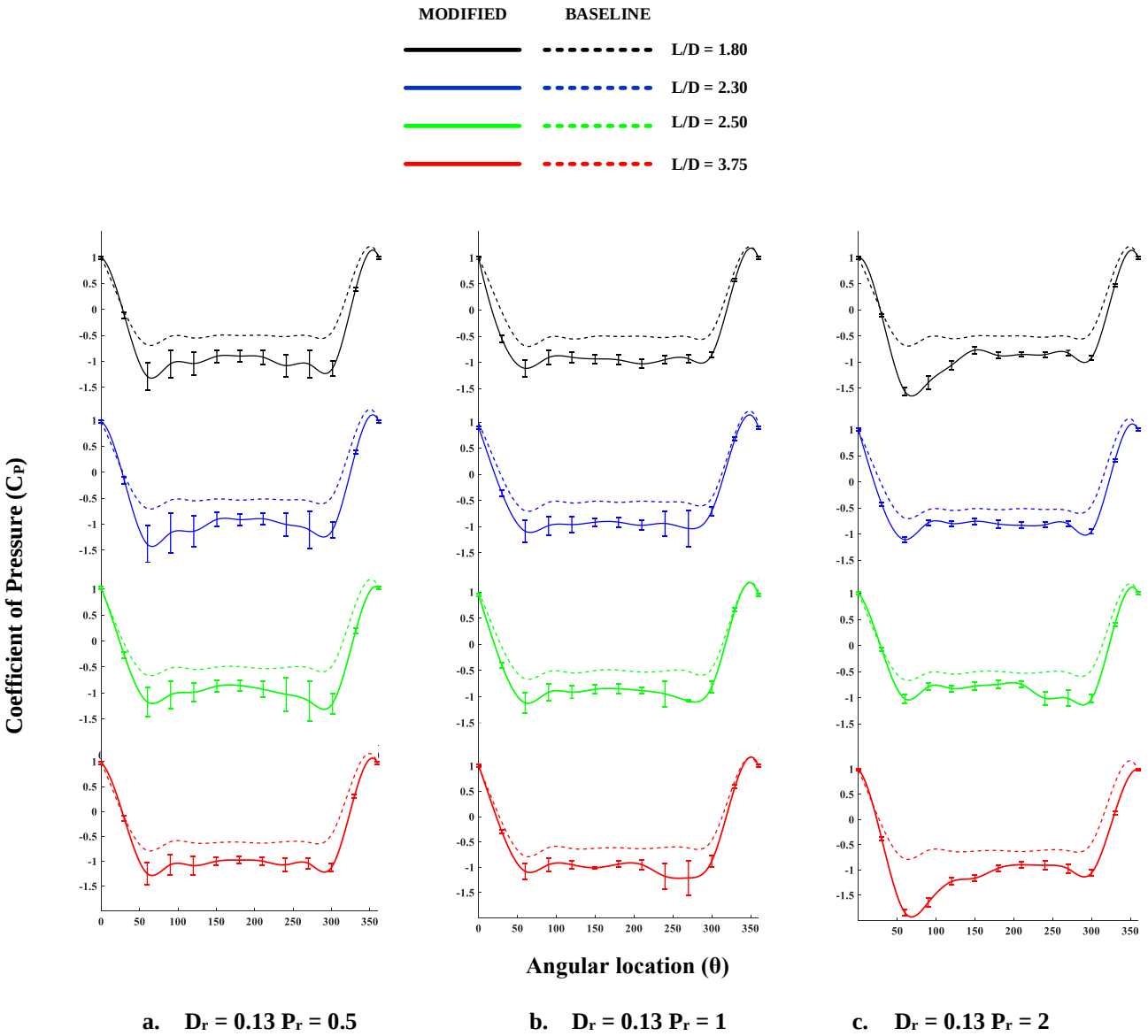

Fig.7 The Coefficient of pressure (C_P) for the baseline (dotted lines) and modified cylinder with strake model (solid line) for D_r= 0.13 along four different spanwise locations L/D =1.80,2.30,2.50 and 3.75 and various Pitch ratios a.) P_r = 0.5, b.) P_r = 1 and c.) P_r = 2

The separation angle is indicated by the intersection of these tangents. In the downstream of the cylinder, it is observed that the pressure increases for the cylinder model with strake by about 23% when compared to that of the base model. When it is

compared with the model for increasing pitch ratio the difference further increases and a maximum of about 32 % increase in the pressure is observed for the modified model with the P_r =2. This is attributed to the decrease in the drag force which can be significantly drawn from Fig.6. Fig.7 depicts the coefficient of pressure for the modified model with D_r = 0.13, at P_r =0.5 the minimum pressure increases for the modified model to that of the baseline model and the separation point shift to a maximum angle for L/D =2.50 and with the increase in the pitch ratio, the increase in the minimum Cp has increased and the flow separation point shift further to a higher angle showcasing a stronger adverse pressure which diffuses with the free stream velocity at a farther angle compared to the baseline model.

B. THE VARIATION OF THE SURFACE PRESSURE COEFFICIENT FOR VARIED DIAMETER RATIO

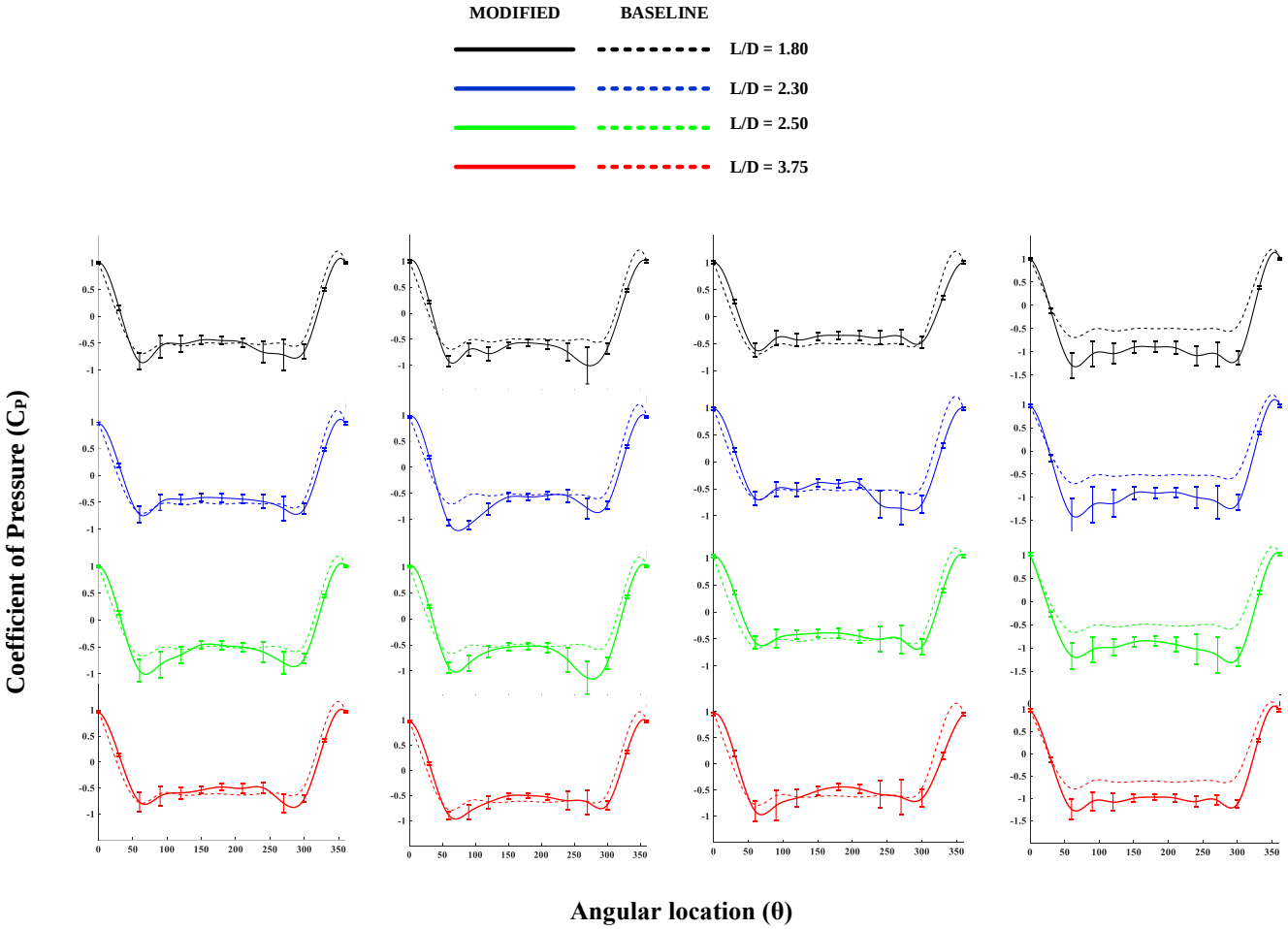

a. D_r = 0.03 P_r = 0.5 **b.** D_r = 0.04 P_r = 0.5 **c.** D_r = 0.1 P_r = 0.5 **d.** D_r = 0.13 P_r = 0.5

Fig.8 The coefficient of pressure for the cylinder model with and without strakes along four different span-wise locations L/D =1.80,2.30,2.50 and 3.75 at constant pitch ratio P_r = 0.5 and various diameter ratios a.) D_r = 0.03, b.) D_r = 0.04, c.) D_r = 0.1, and d.) D_r = 0.13

Fig.8 explains the variation of the surface pressure along the spanwise direction of the cylinder for various diameter ratios at a constant pitch ratio P_r = 0.5. The base model shows a maximum negative pressure of -0.75 and when we see the upstream of the cylinder the pressure changes with the addition of strakes showing an increased slope which reflects the positive favorable pressure gradients for acceleration of the flow. The slope is greater till D_r = 0.1 and for D_r = 0.13 the slope is similar to that of the baseline model. The deacceleration phase is from the point of minimum pressure to the point where the flow gets separated this phase, this phase increases with the increase in the span-wise location. Thus, it refers to the shift in the separation point which again reduces the size of the recirculation bubble at the immediate downstream decreasing the wake region which was earlier identified.

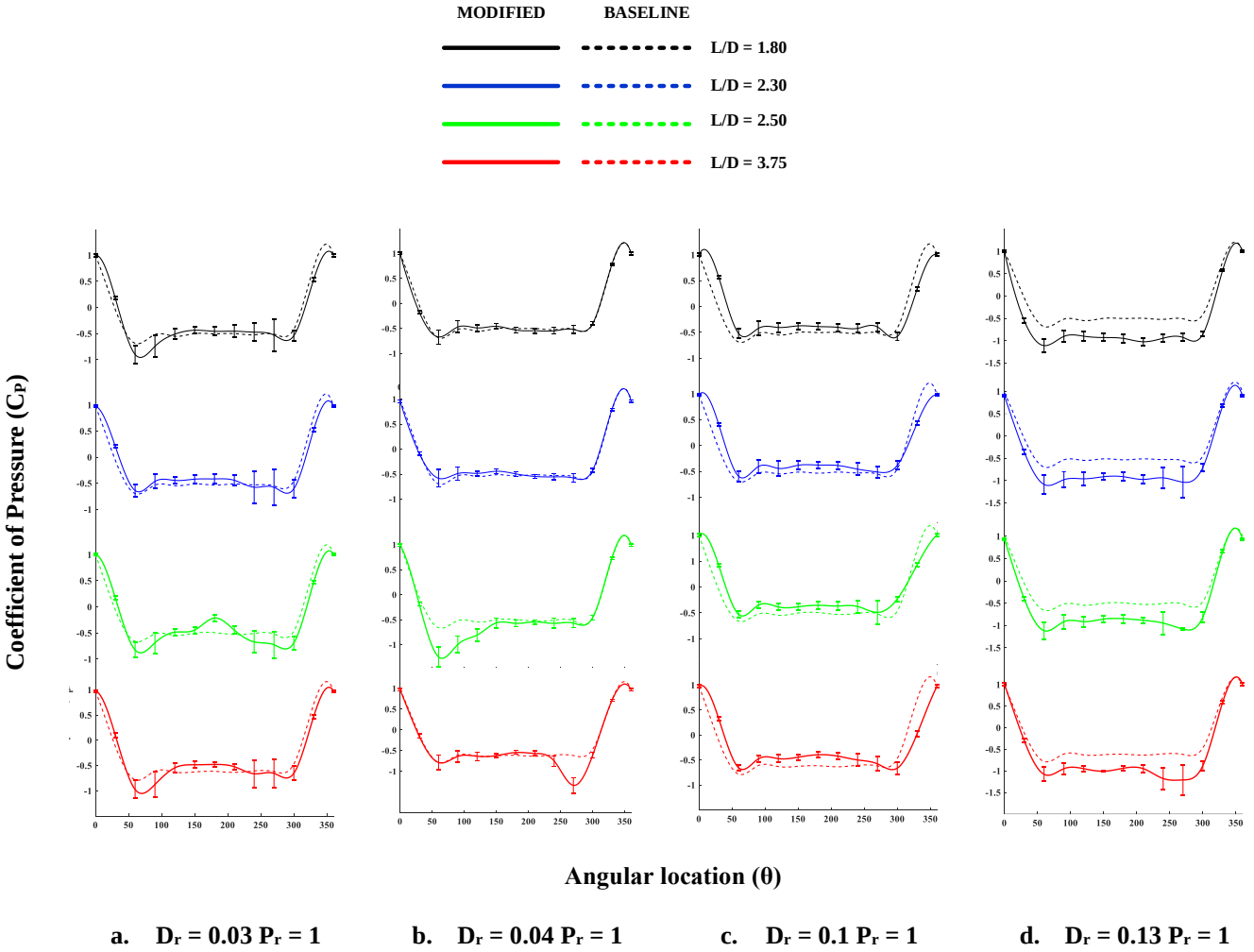

Fig. 9 The coefficient of pressure for the cylinder model with and without strakes along four different span-wise locations L/D =1.80,2.30,2.50 and 3.75 at constant pitch ratio P_r = 1 and various diameter ratios a.) D_r = 0.03, b.) D_r = 0.04, c.) D_r = 0.1, and d.) D_r = 0.13

For the diameter ratio D_r = 0.13, the difference in the pressure for the baseline and the modified model at every angular location is found to be maximum following the same surface pressure trends that of the baseline thus the area of the C_p vs theta increases which reflects the increase in the drag force for the modified model. Fig. 9 explains the variation of the surface pressure along the spanwise direction of the cylinder for various diameter ratios at a constant pitch ratio P_r =1. The coefficient of pressure is almost similar to that of the baseline model for D_r = 0.03 and 0.04. For the D_r = 0.1, we can observe a decrease in the surface pressure for almost all the angular positions which reflects the decrease in drag force, however, there is a significant increase in the surface pressure for the D_r = 0.13. This has ultimately increased the drag coefficient of the model but, the shedding frequency is decreased considerably. The presence of the strake however increases the drag coefficient for D_r = 0.13 but it reduces the intensity of the low-pressure region formed at the immediate downstream of the cylinder.

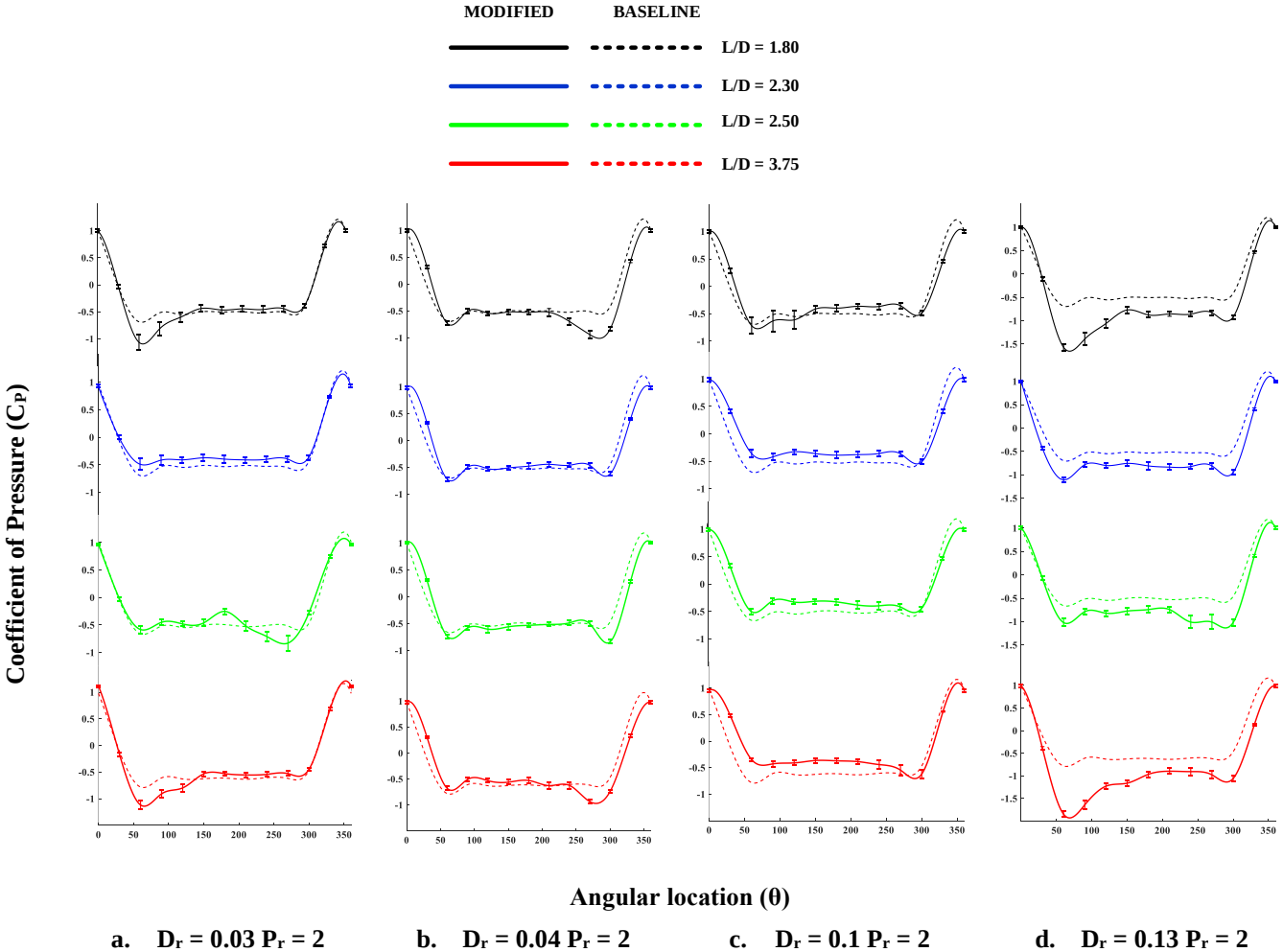

Fig. 10 The coefficient of pressure for the cylinder model with and without strakes along four different span-wise locations L/D =1.80,2.30,2.50 and 3.75 at constant pitch ratio P_r = 2 and various diameter ratios a.) D_r = 0.03, b.) D_r = 0.04, c.) D_r = 0.1, and d.) D_r = 0.13

Similarly, Fig.10 indicates the surface pressure coefficient for the cylinder with various D_r = 0.03,0.04, 0.1 and 0.13 at the constant pressure ratio P_r = 2, the increase in the pressure coefficient value for the D_r = 0.1 seems to be the increase further with the increase in the diameter of the strake and it is limited to the D_r = 0.1 further the pressure coefficient decreases to the maximum value for almost all the angular position. The magnitude is seen to increase with the increase in the pitch ratio. The separation of the flow from the surface of the cylinder seems to shift further away from the angular position of that where the flow got separated from the baseline cylinder. The maximum decrease in the local minimum pressure coefficient for the modified cylinder is seen specifically at L/D 1.80 and L/D =3.75.

C. THE EFFECTS OF VORTEX SHEDDING FOR STRAKES WITH VARIED DIAMETER RATIO AND PRESSURE RATIO:

The cylinder vibrates in the first mode of vibration (as shown by the PSD vs St plots). Amplitudes increase and reach a maximum at the shedding frequency and eventually die down. Lesser order perturbations are elucidated to be unfiltered noise, random temporal fluctuations etc. A plot between the Strouhal number and the PSD of the coefficient of lift is shown below in Fig. 11. The plot shows a distinctive peak in the PSD at a Strouhal number of around 0.17. This is consistent with the theoretical value of around 0.2 for a base cylinder. A similar plot of the PSD of raw pressure data vs Frequency for pressure data obtained from the wake rake can be plotted and is shown in Fig. 11. The maximum peak for the base cylinder model is visible at the Strouhal number (St) of 0.1886, for the cylinder with the D_r =0.03 the Strouhal number of 0.135 for the pitch ratio of 0.5, for the cylinder with the P_r = 1 the Strouhal number of 0.1549 and the for the P_r =2 the Strouhal number of 0.1555 is obtained. The shedding frequency of the cylinder with a strake of Pitch ratios P_r =0.5,1 and 2 is decreased by 28.4%,17% and 17.6% when compared to the baseline cylinder model. When the strake diameter is increased to Dr =0.04 where the Strouhal number corresponding to the pitch ratio P_r of 0.5,1 and 2 is 0.1339,0.1424 and 0.1174. However, the percentage decrease in the shedding frequency for the D_r= 0.04 is approximately 29%,24.5% and 37.75%. The flow structure seems to follow the hypothesis stated [31]. The model with a diameter ratio of 0.1 has shown a Strouhal number of 0.1202 corresponding to a decrease of 36.3 % shedding for a Pitch ratio of 0.5, however, the values for 1 and 2 have attributed to St = 0.1681 and 0.1686 corresponding to a reduction of 10.87 % and 10.60 %. Concerning the max diameter of the strake corresponding to the diameter ratio of 0.13, since it has depicted the maximum pressure difference compared with the baseline model, the shedding frequency has considerably reduced with values of 0.1287, 0.1546 and 0.1549 corresponding to the pitch ratio of 0.5, 1 and 2 thereby projecting the reduction in shedding to around 17.87%,15.45 and 31.76%, which is tabulated in detail in Table III.

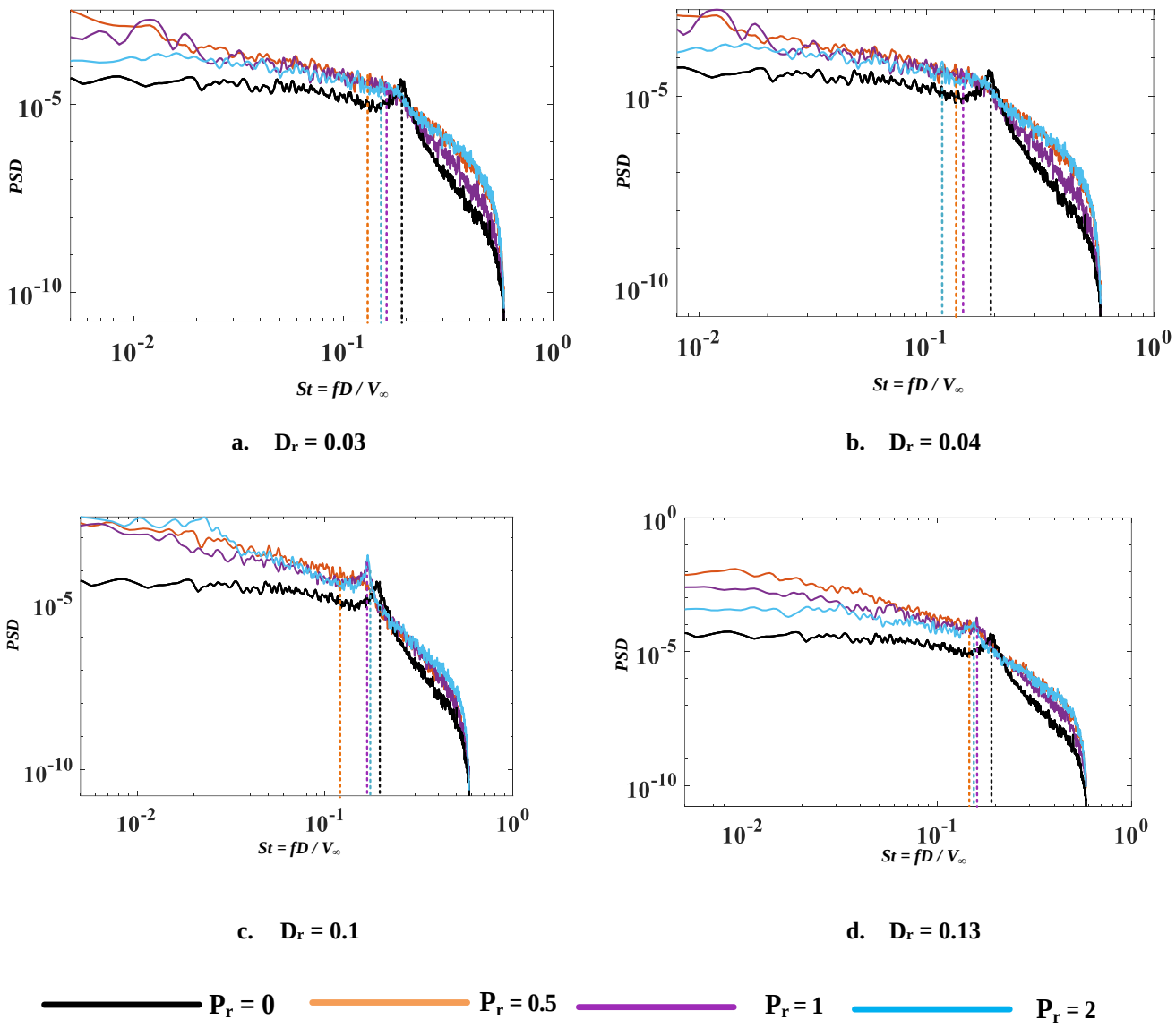

Fig.11 PSD of the time series C_L and respective Strouhal number reflecting the shedding frequencies for the cylinder attached with strakes for various pitch ratios P_r =0,0.5,1 and 2 and various diameter ratios a.) D_r = 0.03 b.) D_r = 0.04 c.) D_r = 0.1 and d.) D_r = 0.13. The colour code represents the strakes with different pitch ratios.

When we see the modified cylinder model shedding characteristics for the model with D_r = 0.1 and P_r = 0.5 has shown a maximum reduction in the Strouhal number reflecting the reduction in shedding of about 36.3% to that of the baseline cylinder model. The frequency is taken in a logarithmic scale for better visualization of the points of inflexion. From the two plots, the following conclusions are drawn. The adequacy of the PSD plot on C_L in the discussion of shedding characteristics can be manifested in the plots as both plots show an inflexion at identical peak values. The plot obtained from the FFT of C_L shows a crisp peak only at the shedding frequency. This concludes that the cylinder in itself is vibrating at the shedding frequency, directly affecting the Coefficients of lift. Fig.12 describes the FFT of time series velocity data at the immediate downstream of

the cylinder for the D_r = 0.03 and 0.04 for three different positions perpendicular to the freestream flow to identify the wake and the variation of the wake profile with the without the presence of the strake. The test section frequency can be inferred and evaluated from the presence of an additional peak in the PSD of wake rake data. The pressure data and hence the PSD of the wake rake show good excitations for ports located near the centerline of the flow. The excitations die down as the port distance from the tunnel wall gets closer. This leads us to an inference that the vortex street is directed towards the centerline and is within the wake regions. It is evident from the plot that the C_L oscillates at a frequency identical to the shedding frequency which concludes that the usage of upstream pressure data is valid in measuring downstream phenomena. Similarly, Fig.13 describes the FFT of time series velocity data at the immediate downstream of the cylinder for the D_r = 0.1 and 0.13 for three different positions perpendicular to the freestream flow to identify the wake and the variation of the wake profile with the without the presence of the strake

Table III Reduction percentage of shedding frequency for a cylinder with strakes of various pitch ratios in comparison with a cylinder without any strakes

D_r	$P_r = 0.5$	$P_r = 1$	$P_r = 2$
0.03	28.4	17	17.6
0.04	29	24.5	35.75
0.1	36.3	10.87	10.60
0.13	31.76	15.43	17.87

Shedding is a complex fluid phenomenon, with an extra-dimensional complexity added due to the Coanda effect produced by the strake. It is demonstrated that shedding in the wake core and wake meandering are two different and independent low-frequency features, with the wake meandering persisting into the intermediate wake and the core shedding traces disappearing early in the near wake. Such low-frequency excitation is seen in Fig. 12 and 13 depicting the flow structure elucidated in the research study [31]. Overall, the presence of the strakes of different diameters and pitches has shown a comparatively lower frequency of shedding compared to the baseline model which is mutually correlated with the PSD obtained from the time series C_L data obtained from the surface pressure data from the cylinder.

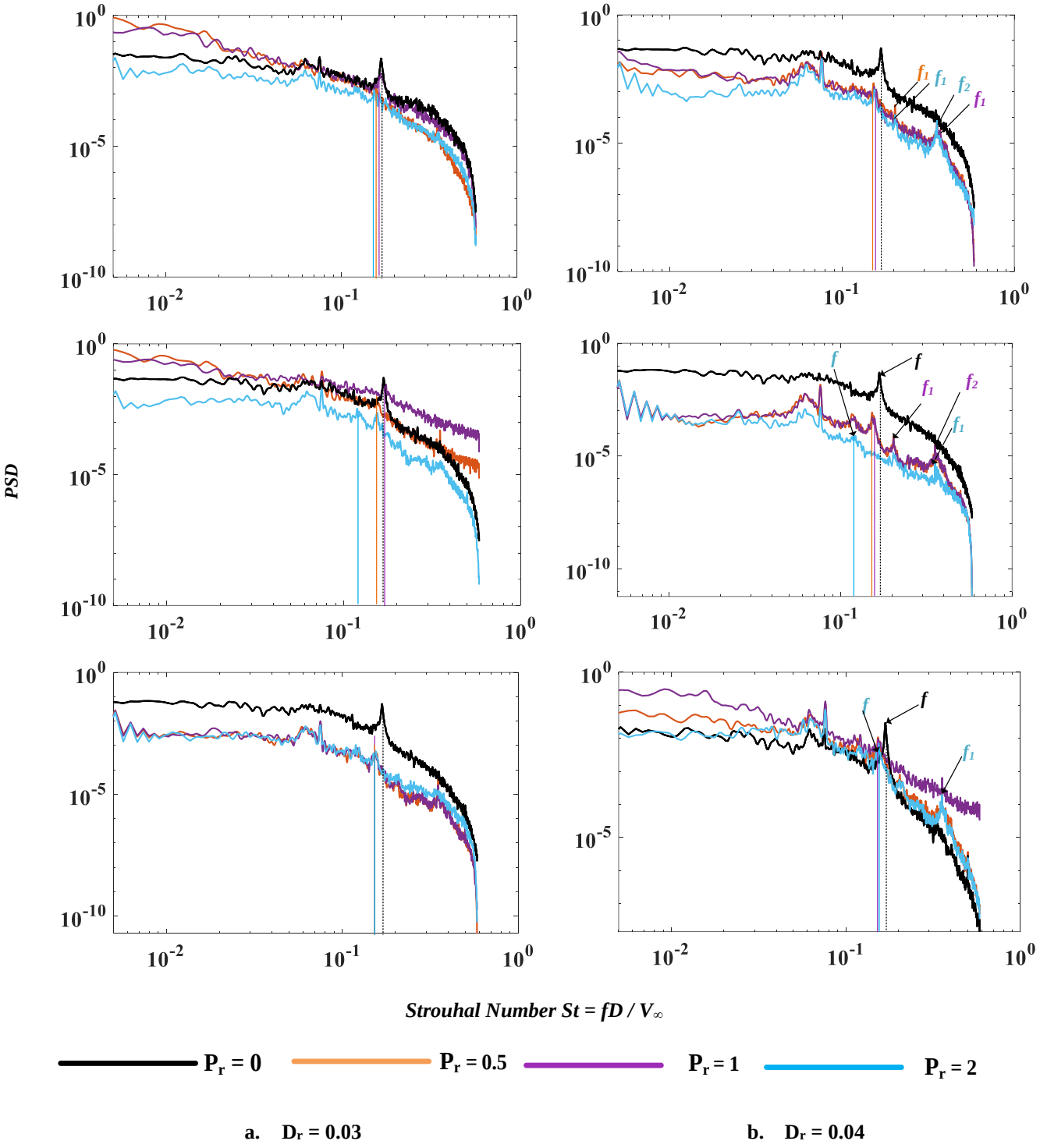

Fig.12 The PSD for the three different positions on the immediate wake region downstream of the cylinder for different pitch ratios (Pr = 0, 0.5,1 and 2 represented by the colour code) for diameter ratio a.) D_r = 0.03 and b.) D_r = 0.04.

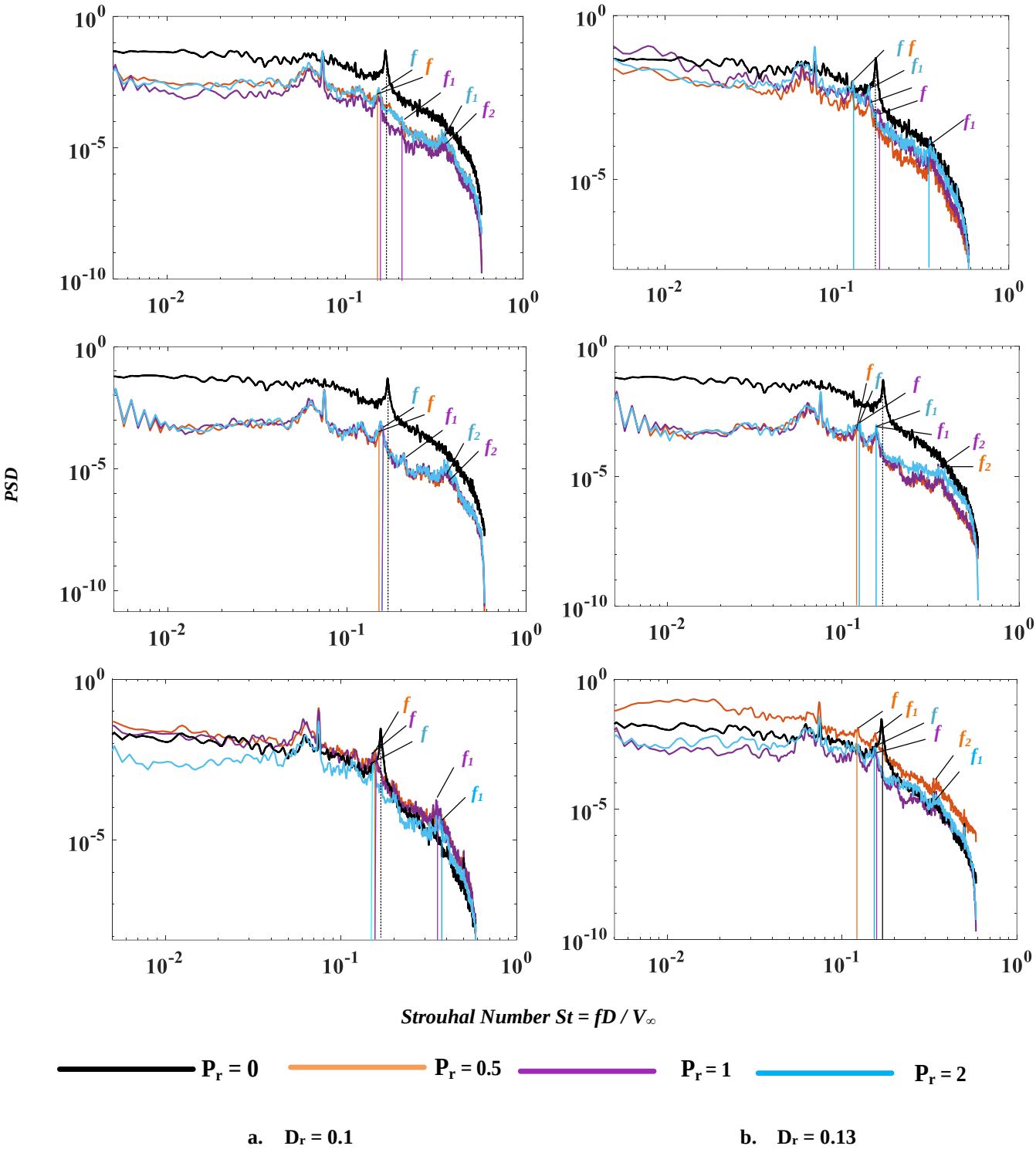

Fig.13 The PSD for the three different positions on the immediate wake region downstream of the cylinder for different pitch ratios (P_r = 0, 0.5,1 and 2 represented by the colour code) for diameter ratio a.) D_r = 0.1 and b.) D_r = 0.13.

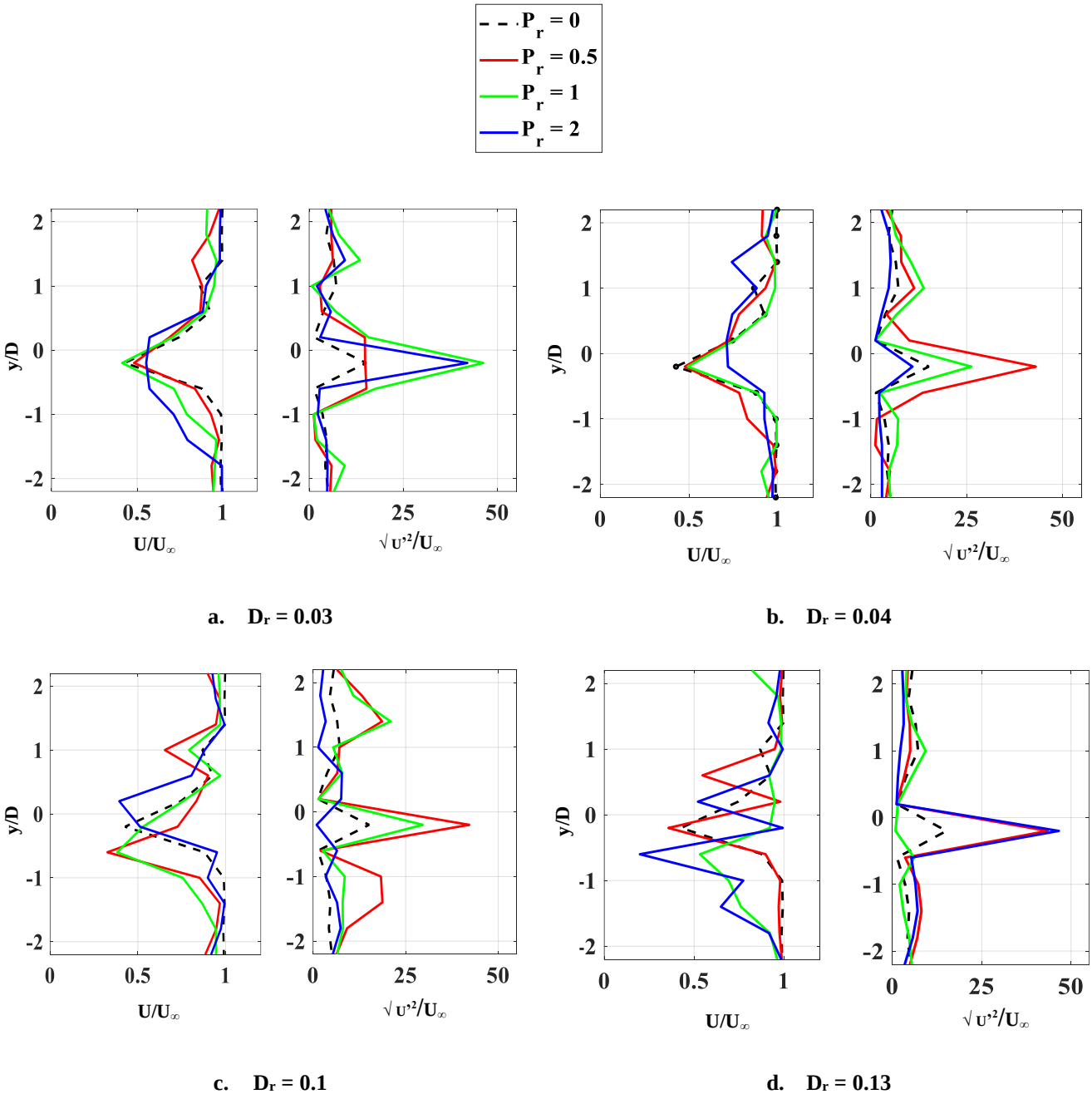

Fig.14 The Velocity profile and the Turbulence intensity (TI) for different pitch ratios (P_r = 0,0.5,1 and 2) where the colour code with dotted line represents the cylinder without any strakes and the solid line represents the cylinder attached with strakes for different diameter ratio a.) D_r = 0.03 b.) D_r = 0.04 c.) D_r = 0.1 and d.) D_r = 0.13.

The PSD from wake velocity has shown the shedding frequencies as well as its harmonics up to the maximum of second-order. The Strouhal number (St) corresponds to the shedding frequency of the cylinder with and without strake and is represented by *f* further, the first harmonics of the shedding frequency is represented by f_1 and the second order harmonics refers to f_2. Fig.14 explores the downstream velocity profile and Turbulence intensity (TI) with the normalized data obtained. The presence of the

strake with the Pitch ratio 0.5 has shown a velocity deficit comparable to that of the baseline model for D_r =0.03 and 0.04 whereas the velocity deficit increases with the increase in the D_r =0.1 and 0.13. The Turbulence increases with the increase in the pitch ratio, it reflects the same way that the increase in diameter ratio has effectively increased the turbulence intensity except for P_r=1 and D_r=0.13.

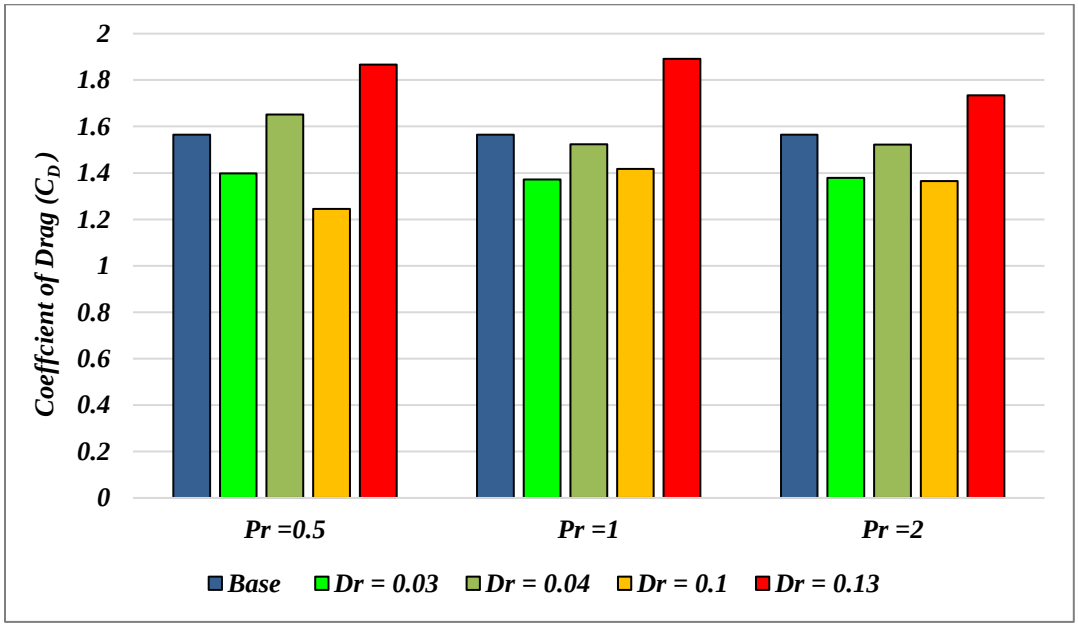

Fig.15 The coefficient of drag (C_D) for the cylinder with different diameter ratios and the pitch ratio. The colour code represents the baseline and the cylinder with varied diameter ratios.

The investigation involved a comparison of the drag coefficients between a cylindrical object fitted with strakes of varying pitch ratios and the unmodified base cylinder. The results showed a substantial reduction in the drag coefficient for the straked cylinders with D_r = 0.03 and 0.1 further at D_r =0.13 it seems to have increased significantly when compared to the unaltered cylinder. The average reduction in the drag coefficient for the cylinder with strake for P_r =0.5, 1 and 2 is around 8.48%, 8.13% and 9.11% respectively, However, keeping the diameter ratio as constant the average reduction of the drag is around 11.61% and 14.19% for the D_r = 0.03 and D_r = 0.1. This reduction percentage was found to be significantly higher, suggesting that the addition of strakes effectively mitigates drag forces. The graphical representations in Fig.15 accompanying the study vividly illustrate these outcomes, serving to elucidate the findings further.

IV. CONCLUSION:

The effects of mitigating the phenomena of Vortex-Induced Vibrations by implementing a circular strake of varying pitch and diameter have been presented. The study has used the time series surface pressure data and the time series velocity profile at the immediate wake of the cylinder to understand the aerodynamic characteristics and the shedding characteristics of the cylinder with and without strake. It is concluded that the reduction in the shedding frequency is well observed for a Diameter ratio above 0.1 and a pitch ratio of 0.5.

1. The presence of a strake has shown a cross-flow along the spanwise direction of the cylinder which has significantly influenced the downstream wake region, which in turn has reduced the shedding of vortices. The Modified model with $P_r = 0.5$ has shown an average reduction in shedding of about 31% for various diameter ratios, whereas, the model with $P_r = 1$ and $P_r = 2$ has shown a reduction of 17% and 20%.
2. The flow structure formed by the presence of a strake has managed to delay the flow separation point by a minimum of 11% to a maximum of 50% which is obtained from the Coefficient of pressure. It is significantly visible for the modified model with $D_r = 0.1$ and $P_r = 0.5$.
3. The presence of the strake with the Pr = 0.5 and Dr = 0.1 on the regular cylinder has shown a maximum reduction in pressure drag of 20.4% compared to that of the base cylinder.
4. The strakes have induced the development of the adverse pressure gradient on the surface of the cylinder making the flow attached over the cylinder further away from the separation point of the baseline model, thereby reducing the energy of the flow downstream and reducing the intensity of the recirculation bubble formed at the immediate wake which is evident from the Turbulence intensity plot which is PSD plot obtained from the downstream velocity discussed above.
5. The influence of the strakes has greatly influenced the downstream flow characteristics and the inbuilt aerodynamics of the structure which is very much evident from the above discussion.

Further Study can be imparted to understand the decay of the vortices from the modified structure at various downstream locations to understand the shedding phenomena in depth.

Nomenclature

C_p	Coefficient of pressure
C_D	Coefficient of drag
C_L	Coefficient of lift

θ	Local inclination angle
P_r	Pitch ratio (pitch/diameter of the cylinder)
D_r	Diameter ratio (diameter of strake /diameter of cylinder)
f, f_1, f_2	Shedding frequency and their harmonics
TI	Turbulence Intensity
VIV	Vortex induced vibration
D	Diameter of the cylinder
d	The diameter of the strakes
PSD	Power spectral density
y/D	Location in the lateral direction perpendicular to the free stream flow
St	Strouhal number
U	Instantaneous velocity at each location downstream of the cylinder
U_∞	Free stream flow velocity
U'	Fluctuation in the velocity
L/D	Span-wise location of pressure ports over the cylinder

ACKNOWLEDGEMENT:

This research work was supported by the Science Engineering Research Board (SERB), Department of Science & Technology (DST), Government of India, File No: CRG/2021/005720.

AUTHORS DECLARATION:

Conflict of Interest

The authors have no conflicts to disclose.

DATA AVAILABILITY:

The data that support the findings of this study are available from the corresponding author upon reasonable request.

REFERENCES:

[1] C.H.K. Williamson, and R. Govardhan, "Vortex-induced vibrations," Annu. Rev. Fluid Mech. **36**(1982), 413–455 (2004).

[2] M. Paidoussis, S. Price, and E. de Langre, "Fluid-Structure Interactions: Cross-Flow-Induced Instabilities," Fluid-Structure Interact. Cross-Flow-Induced Instab., 1–402 (2010).

[3] B. Forouzi Feshalami, S. He, F. Scarano, L. Gan, and C. Morton, "A review of experiments on stationary bluff body wakes," Phys. Fluids **34**(1), 11301 (2022).

[4] C.C. Feng, "The measurement of vortex-induced effects in flow past stationary and oscillating circular and D-section cylinders," (1968).

[5] B. Sharma, G. Verma, and R.N. Barman, “Steady flow of power-law fluids past a slotted circular cylinder at low Reynolds number,” Phys. Fluids **34**(9), 93615 (2022).

[6] L.(王龙军) Wang, M.M.(阿南木) Alam, and Y.(周裕) Zhou, “Drag reduction of a circular cylinder using linear and sawtooth plasma actuators,” Phys. Fluids **33**(12), 124105 (2021).

[7] T.N. Jukes, and K.-S. Choi, “Flow control around a circular cylinder using pulsed dielectric barrier discharge surface plasma,” Phys. Fluids **21**(8), 84103 (2009).

[8] R.F. Huang, C.M. Hsu, and Y.T. Chen, “Modulating flow and aerodynamic characteristics of a square cylinder in crossflow using a rear jet injection,” Phys. Fluids **29**(1), 15103 (2017).

[9] T. Zhou, S.F.M. Razali, Z. Hao, and L. Cheng, “On the study of vortex-induced vibration of a cylinder with helical strakes,” J. Fluids Struct. **27**(7), 903–917 (2011).

[10] D.H. Yeo, and N.P. Jones, “Computational study on aerodynamic mitigation of wind-induced, large-amplitude vibrations of stay cables with strakes,” J. Wind Eng. Ind. Aerodyn. **99**(4), 389–399 (2011).

[11] T.F. Geyer, “Effect of a porous coating on the vortex shedding noise of a cylinder in turbulent flow,” Appl. Acoust. **195**, 108834 (2022).

[12] G. Araujo, J.A. da Silva, and F. Marques, “Energy harvesting from a rotational nonlinear energy sink in vortex-induced vibrations,” J. Fluids Struct. **113**, 103656 (2022).

[13] H. Dai, A. Abdelkefi, and L. Wang, “Vortex-induced vibrations mitigation through a nonlinear energy sink,” Commun. Nonlinear Sci. Numer. Simul. **42**, (2016).

[14] B. Zhang, B. Li, S. Fu, Z. Mao, and W. Ding, “Vortex-Induced Vibration (VIV) hydrokinetic energy harvesting based on nonlinear damping,” Renew. Energy **195**, 1050–1063 (2022).

[15] M. Zeinoddini, A. Farhangmehr, M.S. Seif, and A.P. Zandi, “Cross-flow vortex-induced vibrations of inclined helically straked circular cylinders: An experimental study,” J. Fluids Struct. **59**(1346), 178–201 (2015).

[16] G.R.S. ASSI, P.W. BEARMAN, and J.R. MENEGHINI, “On the wake-induced vibration of tandem circular cylinders: the vortex interaction excitation mechanism,” J. Fluid Mech. **661**, 365–401 (2010).

[17] X. Fu, M. Zhang, S. Fu, B. Zhao, H. Ren, and Y. Xu, “On the study of vortex-induced vibration of a straked pipe in bidirectionally sheared flow,” Ocean Eng. **266**(P3), 112945 (2022).

[18] Y. Hikami, and N. Shiraishi, “Rain-wind induced vibrations of cables stayed bridges,” J. Wind Eng. Ind. Aerodyn. **29**(1–3), 409–418 (1988).

[19] D. Zuo, N.P. Jones, and J.A. Main, “Field observation of vortex- and rain-wind-induced stay-cable vibrations in a three-dimensional environment,” J. Wind Eng. Ind. Aerodyn. **96**(6–7), 1124–1133 (2008).

[20] M. Matsumoto, T. Yagi, Y. Shigemura, and D. Tsushima, “Vortex-induced cable vibration of cable-stayed bridges at high reduced wind velocity,” J. Wind Eng. Ind. Aerodyn. **89**(7–8), 633–647 (2001).

[21] M. Matsumoto, H. Shirato, T. Yagi, M. Goto, S. Sakai, and J. Ohya, “Field observation of the full-scale wind-induced cable vibration,” J. Wind Eng. Ind. Aerodyn. **91**(1–2), 13–26 (2003).

[22] J.B. Jakobsen, T.L. Andersen, J.H.G. Macdonald, N. Nikitas, G.L. Larose, M.G. Savage, and B.R. McAuliffe, “Wind-induced response and excitation characteristics of an inclined cable model in the critical Reynolds number range,” J. Wind Eng. Ind. Aerodyn. **110**, 100–112 (2012).

[23] H.(胡浩) Hu, W.(赵伟文) Zhao, and D.(万德成) Wan, “Vortex-induced vibration of a slender flexible riser with grooved and spanwise strips subject to uniform currents,” Phys. Fluids **34**(12), 125131 (2022).

[24] T. Ishihara, and T. Li, “Numerical study on suppression of vortex-induced vibration of circular cylinder by helical wires,” J. Wind Eng. Ind. Aerodyn. **197**(December 2019), 104081 (2020).

[25] C.(马春卉) Ma, W.(赵伟文) Zhao, and D.(万德成) Wan, “Numerical investigations of the flow-induced vibration of a three-dimensional circular cylinder with various symmetric strips attached,” Phys. Fluids **34**(6), 65102 (2022).

[26] S. Arunvinthan, S. Nadaraja Pillai, and S. Cao, “Aerodynamic characteristics of variously modified leading-edge protuberanced (LEP) wind turbine blades under various turbulent intensities,” J. Wind Eng. Ind. Aerodyn. **202**, 104188 (2020).

[27] E. Livya, and S. Nadaraja Pillai, “Effect of turbulence intensity on aerodynamic characteristics of extended trailing edge airfoil,” Aircr. Eng. Aerosp. Technol. **94**(10), 1780–1791 (2022).

[28] J.D. Anderson, *Fundamentals of Aerodynamics (6th Edition)* (2011).

[29] A. Sundaresan, S. Arunvinthan, A.A. Pasha, and S.N. Pillai, “Effect of Ice accretion on the aerodynamic characteristics of wind turbine blades,” Wind Struct. An Int. J. **32**(3), 205–217 (2021).

[30] S. Ramalingam, R.F. Huang, and C.M. Hsu, “Effect of crossflow oscillation Strouhal number on circular cylinder wake,” Phys. Fluids **35**(9), (2023).

[31] A. Piqué, M.A. Miller, and M. Hultmark, “Dominant flow features in the wake of a wind turbine at high Reynolds numbers,” J. Renew. Sustain. Energy **14**(3), (2022).